Springer

KSME

Journal of Mechanical Science and Technology 29 (3) (2015) 1307~1318
www.springerlink.com/content/1738-494x
DOI 10.1007/s12206-015-0246-3

Effect of circular cylinder location on three-dimensional natural convection in a cubical enclosure †

Changyoung Choi[1], Hyun Woo Cho[1], Man Yeong Ha[1,*] and Hyun Sik Yoon[2]

[1]*School of Mechanical Engineering, Pusan National University, Jang Jeon 2-Dong, Geum Jeong Gu, Busan, 609-735, Korea*
[2]*Global Core Research Center for Ships and Offshore Plants, Pusan National University, Jang Jeon 2-Dong, Geum Jeong Gu, Busan, 609-735, Korea*

(Manuscript Received May 19, 2014; Revised August 25, 2014; Accepted December 4, 2014)

Abstract

This paper presents the results of immersed boundary method-based three-dimension numerical simulations of natural convection in a cubical enclosure with an inner circular cylinder at a Prandtl number of 0.7. This simulation spans three decades of Rayleigh number, Ra, from 10^3 to 10^6. The location of the inner circular cylinder is changed vertically along the centerline of the cubical enclosure. This study primarily focuses on the effects of both buoyancy-induced convection and the location of the inner circular cylinder on heat transfer and fluid flow in the cubical enclosure. In the range of Rayleigh numbers considered in this study, the thermal and flow fields eventually reach steady state, regardless of the location of the inner cylinder. When Ra is 10^3, the end wall of the cubical enclosure has a negligible effect on the thermal and flow fields in the enclosure. However, in the range of $10^4 \le Ra \le 10^6$, the effect of the end wall on heat transfer and fluid flow in the enclosure depends on both the location of the inner cylinder and the Rayleigh number. Detailed analysis results for the distribution of streamlines, isotherms, and Nusselt numbers are presented in this paper.

Keywords: Natural convection; Immersed boundary method; Low-temperature cubical enclosure; High-temperature inner circular cylinder; Effect of cylinder location

1. Introduction

Natural convection in an enclosure is relevant to many industrial applications and tools, such as heat exchangers, nuclear and chemical reactors, and cooling of electronic equipment. Natural convection heat transfer exhibits a great variety of complex dynamic behaviors, which depend greatly on the geometry and thermal conditions of the enclosure. Many investigations have addressed the influence of various thermal conditions on natural convection in an enclosure without an inner body [1-5]. However, natural convection in an enclosure containing an inner body filled with convective fluid is more complex and applicable to engineering than a simple enclosure without an inner body. Thus, many researchers have studied natural convection in an enclosure that includes an inner body [6-10].

In the past few years, many researchers have investigated the effects of various parameters on natural convection in an enclosure with an inner body. For example, Cesini et al. [6] investigated the influence of the aspect ratio of an enclosure on natural convection in the enclosure. Shu and Zhu [7] and Angeli et al. [8] studied the effect of diameter-to-side aspect ratio, and Kim et al. [9] studied the effect of the position of an inner cylinder on natural convection in the space between a cylinder and an enclosure. Xu et al. [10] reported changes in the characteristics of natural convection in an enclosure with respect to the shape of the inner body.

Cesini et al. [6] performed numerical and experimental analyses for natural convection heat transfer between an inner cylinder and a rectangular enclosure. The study investigated the effects of the Rayleigh number, Ra, and the aspect ratio of an enclosure on the heat transfer between the cylinder and the enclosure. The range of the Rayleigh number and aspect ratio under consideration were $1.3\times10^3 \le Ra \le 7.5\times10^4$ and 2.1, 2.9, 3.6, and 4.3, respectively. As the Rayleigh number increased, the average heat transfer coefficient increased, and the maximum value was found at a low aspect ratio.

Shu and Zhu [7] studied the changes in the thermal and flow fields in a square enclosure with respect to the various radii of an inner circular cylinder. They obtained the results for a Rayleigh number range of $10^4 \le Ra \le 10^6$ with a Prandtl number of 0.71 and diameter-to-side aspect ratios between 1.67 and 5.0. It was found that both the diameter-to-side aspect ratio and the Rayleigh number are critical to the patterns of thermal and flow fields in the enclosure.

Angeli et al. [8] investigated the effect of the radius of an

*Corresponding author. Tel.: +82 51 510 2440, Fax.: +82 51 515 3101
E-mail address: myha@pusan.ac.kr
† Recommended by Associate Editor Ji Hwan Jeong

inner cylinder on the heat transfer between a cylinder and a square enclosure. The range of the Rayleigh number was $10^2 \le Ra \le 5\times10^6$, and the Prandtl number was 0.7. Four values of the diameter-to-side ratio were considered: 0.2, 0.4, 0.6, and 0.8. Substantial differences were observed in the thermal and flow fields in the square enclosure, depending on the diameter-to-side aspect ratio and the Rayleigh number.

Kim et al. [9] studied natural convection in a square enclosure with respect to the position of the inner circular cylinder. The range of the Rayleigh number was $10^3 \le Ra \le 10^6$, and the Prandtl number was 0.7. The inner circular cylinder moved along the vertical centerline of the enclosure in the range of $-0.25 \le \delta \le 0.25$. They reported that the number, size, and formation of convection cells in the enclosure depend on the location of the inner cylinder as well as the Rayleigh number.

Xu et al. [10] investigated the effect of the shape of an inner cylinder on natural convection in an enclosure by changing the cross-sectional shape of the inner cylinder to square, rhombic, circular, and triangular. The range of the Rayleigh number was $10^3 \le Ra \le 10^7$, and the Prandtl number was 0.7. They reported that the characteristics of thermal and flow fields in an enclosure are changed by the shape of the cross section of the inner cylinder.

Most of these previous studies have investigated natural convection in an enclosure by using the two-dimensional computational domain, which assumes that the enclosure has an infinite length. However, natural convection in a three-dimensional space such as a cubical enclosure cannot be properly analyzed by a two-dimensional simulation, as reported by Chan and Banerjee [11]. Thus, three-dimensional analysis has been conducted by many researchers for cubical enclosures without an inner body [11-13] or with an inner body [14, 15].

Chan and Banerjee [11] investigated natural convection in a hexagonal enclosure by changing the aspect ratio of the enclosure to 1:1 and 5:11. The Rayleigh number was 10^4, and the Prandtl number was 0.72. They compared the results of two-dimensional and three-dimensional simulations and found that two-dimensional calculation does not agree well with three-dimensional calculation, especially for enclosures with an aspect ratio less than unity.

Fusegi et al. [12] studied three-dimensional steady natural convection in a cubical enclosure without an inner body. The cubical enclosure was heated differentially at two vertical sidewalls. The range of the Rayleigh number was $10^3 \le Ra \le 10^6$, and the Prandtl number was 0.71. It was found that as the Rayleigh number increased, the convective activities intensify and significant variations in the z-direction are confined to narrower areas close to the end walls.

Pallares et al. [13] performed three-dimensional analysis to characterize natural convection in a cubical enclosure in which buoyancy was induced by imposing a moderate temperature difference between the heated bottom and cooled top plates with perfectly adiabatic vertical walls, in the range of $3{,}500 \le Ra \le 10{,}000$ at a Prandtl number of 0.71. They reported that there are four different thermal and flow structures and that the surface-averaged Nusselt number depends on these structures.

Ha and Jung [14] investigated natural convection in a cubical enclosure with an inner cubic body. They conducted numerical simulation to investigate three-dimensional, steady, conjugate heat transfer in a cubical enclosure with a heat-conducting cubic body. The range of the Rayleigh number was $10^3 \le Ra \le 10^5$, and the Prandtl number (Pr) was 0.0112. They reported that the flow and isotherm distributions change to complex three-dimensional patterns as the Rayleigh number increases.

Yoon et al. [15] studied the influence of the position of an inner sphere on natural convection in a cubical enclosure. They investigated the effect of the location of the inner sphere on the heat transfer and fluid flow in a cubical enclosure in the Rayleigh number range of $10^3 \le Ra \le 10^6$. They reported that the distribution of the local Nusselt number of the cylinder depends greatly on the location of the inner sphere as well as the Rayleigh number.

As shown in the results of previous studies, natural convection in an enclosure depends on the shape and position of an inner body. Additionally, the thermal and flow characteristics of natural convection in a cubical enclosure cannot be properly analyzed by a two-dimensional simulation. However, there is little information about three-dimensional natural convection when a circular cylinder exists in different positions in a cubical enclosure. The configuration of the cubical enclosure with an inner circular cylinder which has the same length as the enclosure is widely present in the engineering equipment such as shell-and-tube heat exchangers, underground transmission line and cask for keeping the nuclear wastes. In these devices, the mutual position between the enclosure and the inner cylinder is one of the key design parameters. Thus, this study investigates the effect of the position of an inner circular cylinder on three-dimensional natural convection in a cubical enclosure. Isotherms, streamlines, and Nusselt number are presented to analyze the effect of the position of the cylinder on natural convection in the cubical enclosure.

2. Computational details

2.1 Numerical methods

To investigate the effect of the position of an inner cylinder on natural convection in an enclosure, Kim et al. [9], Lee et al. [16], Kang et al. [17], Yoon et al. [18], and Park et al. [19] used the immersed boundary method (IBM). When the location of an inner circular cylinder is changed in a cubical enclosure, the IBM is easier to implement and more efficient than classical approaches such as body-fitted curvilinear grids. Especially, when the circular cylinder is very close to the wall of the enclosure, the grid generation is not easy due to the high aspect ratio and the limitation of the number of grids. However, when the IBM used to generate grid for the configuration which the distance between the circular cylinder and the wall

of the enclosure is very small, it is easy to apply the dense grids without the huge increase in the number of grids. Thus, in this study, the IBM was used to handle the surface of the circular cylinder located in the cubical enclosure.

The governing equations for mass, momentum, and energy conservation using the IBM are defined as follows in their nondimensional forms:

$$\frac{\partial u_i}{\partial x_i} - q = 0 , \tag{1}$$

$$\frac{\partial u_i}{\partial t} + u_j \frac{\partial u_i}{\partial x_j} = -\frac{\partial p}{\partial x_i} + Pr \frac{\partial^2 u_i}{\partial x_j \partial x_j} + Ra Pr \theta \delta_{i2} + f_i , \tag{2}$$

$$\frac{\partial \theta}{\partial t} + u_j \frac{\partial \theta}{\partial x_j} = \frac{\partial^2 \theta}{\partial x_j \partial x_j} + h . \tag{3}$$

The dimensionless variables in the preceding equations are defined as

$$t = \frac{t^* \alpha}{L^2},\ x_i = \frac{x_i^*}{L},\ u_i = \frac{u_i^* L}{\alpha},\ p = \frac{p^* L^2}{\rho \alpha^2},\ \theta = \frac{T^* - T_c^*}{T_h^* - T_c^*} . \tag{4}$$

In the preceding equations, ρ, T, and α represent the density, dimensional temperature, and thermal diffusivity, respectively. The superscript * in Eq. (4) represents the dimensional variables; x_i represents Cartesian coordinates, u_i represents the corresponding velocity components, t is the time, p is the pressure, and θ is the temperature.

The preceding nondimensionalization produces two dimensionless parameters: $Pr = \nu / \alpha$ and $Ra = g\beta L^3 \left(T_h^* - T_c^* \right) / \nu\alpha$, where ν, g, and β are the kinematic viscosity, gravitational acceleration, and volume expansion coefficient, respectively. The terms of q, f_i, and h in Eqs. (1)-(3) are related to the IBM. The mass source/sink, q, in Eq. (1) and momentum force, f_i, in Eq. (2) were applied to the surface or inside the body to satisfy the no-slip condition and mass conservation in the cell containing the immersed boundary. In Eq. (3), the heat source/sink, h, was applied to satisfy the isothermal boundary condition on the surface of the inner body. A second-order linear or bilinear interpolation scheme was applied to satisfy the no-slip and isothermal conditions on the immersed boundary. Kim et al. [20] and Kim and Choi [21] provide further details of the IBM.

The semi-implicit scheme was used for the temporal and spatial discretization of governing Eqs. (1)-(3). Thus, the advection terms were treated explicitly using the second-order Adams-Bashforth scheme, and the diffusion terms were treated implicitly using the second-order accurate Crank-Nicolson scheme. The discrete governing equations in conservative form are as follows:

$$\frac{u_i^{n+1} - u_i^n}{\Delta t} = -\frac{3}{2} NL(u_i^n) + \frac{1}{2} NL(u_i^{n-1}) - \frac{\partial P^n}{\partial x_i} + \frac{1}{2} Pr \left[DIF(\mathrm{u}_i^{n+1}) + DIF(u_i^n) \right] + RaPr\theta^n \delta_{i2} + f_i , \tag{5}$$

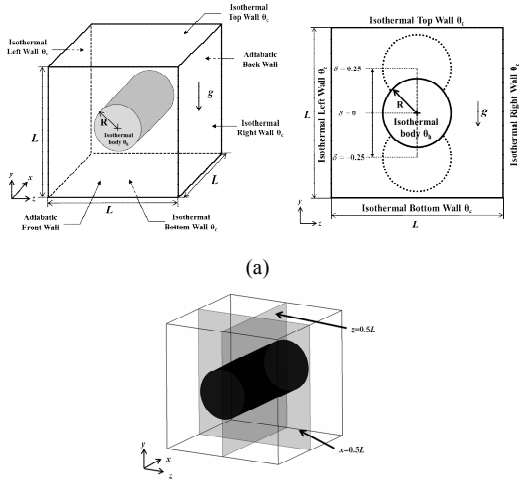

(a)

(b)

Fig. 1. (a) Computational domain and coordinate system along with boundary conditions; (b) definition of planes for cross-sectional view.

$$\frac{\theta^{n+1} - \theta^n}{\Delta t} = -\frac{3}{2} NL(\theta^n) + \frac{1}{2} NL(\theta^{n-1}) + \frac{1}{2} \left[DIF(\theta^{n+1}) + DIF(\theta^n) \right] + h . \tag{6}$$

The term $NL(\varphi)$ and $DIF(\varphi)$ in these equations are defined as

$$NL(\varphi_i) = \frac{\partial u_j \varphi_i}{\partial x_j},\quad DIF(\varphi_i) = \frac{\partial^2 \varphi_i}{\partial x_j \partial x_j} . \tag{7}$$

The basic method for the discretization of the partial differential equations was the finite volume method. A time interval to obtain a Courant-Friedrichs-Lewy (CFL) number smaller than 0.15 was selected in this study for the temporal integration in the time-marching procedure. To efficiently calculate the three-dimensional governing equations, the message passing interface (MPI) parallel computing method was used in this study.

Once the velocity and temperature fields are obtained, the local and surface-averaged Nusselt numbers, Nu and $\overline{Nu}$, are defined, respectively, as

$$Nu = \left. \frac{\partial \theta}{\partial n} \right|_{wall},\quad \overline{\mathrm{Nu}} = \frac{1}{A} \int Nu\ dA \tag{8}$$

where n is the normal direction with respect to the wall and A is the area of the surface of the cylinder.

2.2 Computational conditions

A schematic of the system considered in this study is shown in Fig. 1(a). The edge length of the enclosure is L, and the

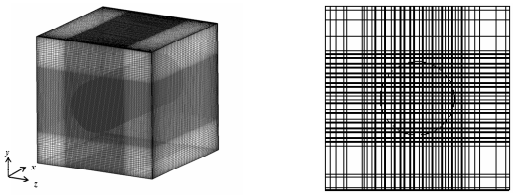

(a) (b)

Fig. 2. (a) Typical three-dimensional view; (b) two-dimensional (y, z) -plane view at $x = 0.5L$ for $\delta = 0$ with nonuniform grid distribution denoting the immersed boundary for inner circular cylinder.

radius of the inner circular cylinder is $R = 0.2L$. To represent the location of the inner circular cylinder along the vertical centerline of the cubical enclosure, the dimensionless location of the inner circular cylinder, δ ($Ra = 10^3$), varies within the range $-0.25 \le \delta \le 0.25$. Ra varies in the range of $10^3 \le Ra \le 10^6$, and Pr is 0.7. No-slip and impermeability conditions were used for the walls of the enclosure and the surface of the inner cylinder. The front and back walls of the cubical enclosure were assumed to be perfectly insulated, and the other walls of the cubical enclosure were assumed to be isothermal, with nondimensional temperature $\theta_c = 0$. The surface of the inner circular cylinder was also assumed to be isothermal, with nondimensional temperature $\theta_h = 1$. The Boussinesq approximation accounted for density variations and gravitational acceleration acted in the negative y-direction.

In the computational domain of the cubical enclosure, the grid points were nonuniformly distributed, as shown in Fig. 2. The distribution of grid points was dense around the walls of the enclosure and cylinder to account for the high gradients. The dense grids were uniformly distributed within the cylinder. The minimum size of the grid was $L / 250$, and the maximum size of the grid was $3L / 200$. For the process of grid distribution between the minimum and maximum sizes, the hyperbolic tangent function was used. Grid independence of the resolution was tested by additional simulations on much finer grids, up to the minimum mesh size of $L / 350$. The difference in the surface-averaged Nusselt number of the enclosure and cylinder obtained by using the coarse and fine grids was less than 0.3%.

2.3 Validation test

To verify the present numerical methods, the case of natural convection in a rectangular enclosure with an inner circular cylinder, as reported by Fiscaletti et al. [22], was considered. In the process of the validation test, we followed their experimental conditions. The rectangular enclosure is filled with water, and the thermal boundary conditions are assumed to be isothermal, with low and high temperatures for the surfaces of the enclosure and cylinder, respectively.

Fig. 3 shows a comparison of the surface-averaged Nusselt number, $\overline{Nu}_c$, computed by the present numerical methods

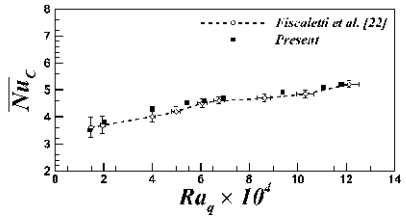

Fig. 3. Comparison of the present surface-averaged Nusselt numbers with those obtained by Fiscaletti et al. [22].

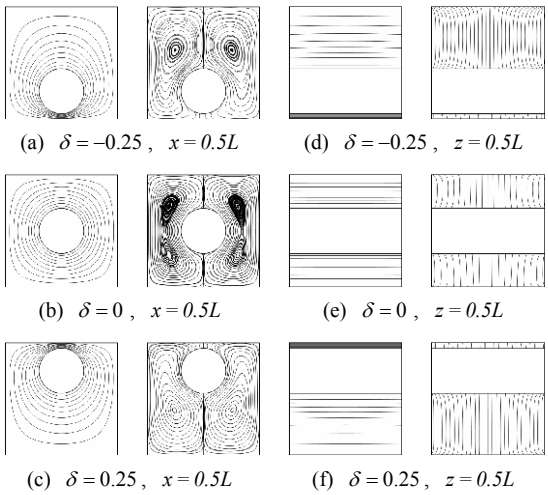

Fig. 4. Isothermals and streamlines for different δ values at $Ra = 10^3$ (contour values range from 0.1 to 1 with 10 levels).

with the experimental data obtained by Fiscaletti et al. [22]. The definitions of $\overline{Nu}_c$ and Ra used in this validation test were the same as those used by Fiscaletti et al. [22]. As shown in Fig. 3, the $\overline{Nu}_c$ values obtained from the present numerical results generally agree with the experimental results obtained by Fiscaletti et al. [22].

3. Results

3.1 Thermal and flow fields

3.1.1 $Ra = 10^3$

Fig. 4 shows the distribution of the isotherms and streamlines when the inner cylinder moves downward and upward at $Ra = 10^3$. The dependence of the thermal and flow fields in the cubical enclosure on δ can be observed in the plots of the isotherms and streamlines for different δ values at $Ra = 10^3$, as shown in Fig. 4. The definitions for the x- and z-plane cross sections of the enclosure are given in Fig. 1(b).

When the inner circular cylinder is located at the lowest position of $\delta = -0.25$, two overall rotating main eddies are formed at the left and right sides of the x-plane cross section of the enclosure, as shown in Fig. 4(a). When $\delta = -0.25$, the centers of the inner vortices are located over the upper surface of the circular cylinder owing to the wider space available between the inner circular cylinder and the top wall of the cubical enclosure. This wide space ensures the strong circula-

tion of flow.

As shown in Fig. 4(b), when the inner circular cylinder is positioned at the center of the cubical enclosure, the thermal and flow fields are almost symmetrical about the vertical and horizontal centers of the cubical enclosure. When $\delta = 0$, there are two inner vortices in each main circulation area in the upper and lower parts of the x-plane cross sections of the enclosure.

When the value of δ is higher than 0, the size of the lower inner vortex is larger than that of the upper vortex because the wide space available between the cylinder and the bottom wall of the enclosure enlarges the circulation of the lower inner vortex. When the circular cylinder moves continuously upward to $\delta = 0.25$, as shown in Fig. 4(c), the inner vortices in the main circulation areas are located below the center of the lower surface of the cylinder.

Even though the thermal and flow fields on the x-plane cross section of the enclosure depend on the dimensionless location of the cylinder, δ, the effect of δ on the three-dimensionality in the thermal and flow fields of the z-plane cross section of the enclosure is negligible, as shown in Figs. 4(d)-(f). This is because, at this low Rayleigh number of 10^3, the effect of convection on the thermal and flow fields in the cubical enclosure is so small that the effects of the front and back adiabatic walls on the thermal and flow fields are negligible, as shown in the plots of the z-plane cross section in Figs. 4(d)-(f).

3.1.2 $Ra = 10^4$

Fig. 5 shows the thermal and flow fields in the cubical enclosure with respect to the dimensionless location of the cylinder, δ, at $Ra = 10^4$. The effect of convection on heat transfer in the cubical enclosure at $Ra = 10^4$ is greater than that at $Ra = 10^3$. Thus, when $\delta = -0.25$, a weak upward thermal plume appears over the upper surface of the circular cylinder for $Ra = 10^4$, unlike that for $Ra = 10^3$, as shown in Figs. 4(a) and 5(a).

When the circular cylinder is located at the center of the enclosure, $\delta = 0$, the upward thermal plume becomes weak owing to the decrease in the space between the cylinder and the wall of the enclosure. However, a careful observation shows that the thermal boundary layer on the bottom of the circular cylinder is thinner than that on the top of the circular cylinder. This is because the effect of convection on thermal and flow fields increases when the Rayleigh number increases. Even though the effect of convection on heat transfer in the enclosure increases as the Rayleigh number increases, the thermal and flow fields on the x-plane cross section of the enclosure for $\delta = 0$ and $Ra = 10^4$ are almost the same as those for $\delta = 0$ and $Ra = 10^3$, as shown in Figs. 4(b) and 5(b). Thus, when the circular cylinder is located at the vertical center of the cubical enclosure, the effects of the front and back adiabatic walls of the cubical enclosure on the thermal and flow fields are negligible when $Ra = 10^4$.

As the circular cylinder moves upward to $\delta = 0.25$, the two inner vortices in each main circulation area of the x-plane cross section of the enclosure merge and generate one inner vortex in each main circulation area, as shown in Fig. 5(c). When the circular cylinder is located close to the top wall of the enclosure, a stagnation region with cold, heavy fluid is formed in the lower half of the enclosure because the strong convective flow is confined in the upper half of the enclosure. Thus, at $\delta = 0.25$, the heat transfer at the bottom wall of the enclosure is not effective, as shown in Fig. 5(c).

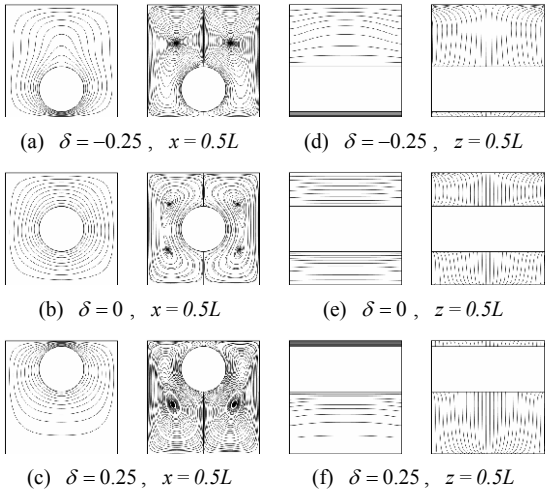

Fig. 5. Isothermals and streamlines for different δ values at $Ra = 10^4$ (contour values range from 0.1 to 1 with 10 levels).

Because the convection effect becomes greater at $Ra = 10^4$, the thermal and flow fields on the z-plane cross section of the enclosure are influenced by the position of the circular cylinder, as shown in Figs. 5(d)-(f). When $\delta = -0.25$, a thermal plume is observed on the z- and x-plane cross sections of the enclosure, as shown in Figs. 5(a) and (d). However, when the circular cylinder is located at the center of the enclosure, $\delta = 0$, the effect of convection is negligible on the thermal and flow fields of the z-plane cross section of the enclosure, as shown in Fig. 5(e). As the circular cylinder moves upward through the vertical center of the enclosure, there is a weak upward thermal plume at the bottom wall of the enclosure, as shown in Fig. 5(f). Because thermal convection is mainly generated by the inner high-temperature circular cylinder, the flow diverges at the center of the top wall of the enclosure and converges at the center of the bottom wall of the enclosure, as shown in Figs. 5(d) and (f). Thus, the direction of the thermal plume at $\delta = 0.25$ is upward from the bottom wall of the enclosure, as shown in Fig. 5(f).

3.1.3 $Ra = 10^5$

Fig. 6 shows the distribution of isotherms and streamlines for different δ values at $Ra = 10^5$. The pattern of thermal and flow fields on the x- and z-plane cross sections of the enclosure at $Ra = 10^5$ is significantly different from that at lower Rayleigh numbers of $Ra = 10^3$ and 10^4. This is because when Ra is 10^5, buoyancy-induced convection be-

comes more predominant than the conduction of heat transfer between the cylinder and the enclosure.

When the inner circular cylinder is located at the lowest position of $\delta = -0.25$, the size of the thermal plume on the x-plane cross section of the enclosure for $Ra = 10^5$ is larger than that for $Ra = 10^4$, as shown in Figs. 5(a) and 6(a). The large thermal plume over the upper surface of the circular cylinder creates a strong thermal gradient on the top wall of the cubical enclosure.

As shown in Figs. 5(b) and 6(b), when the circular cylinder is placed at the vertical center of the enclosure, $\delta = 0$, there is a thermal plume over the upper surface of the cylinder for $Ra = 10^5$, unlike that for $Ra = 10^4$. This thermal plume produces a strong thermal gradient at the top wall of the cubical enclosure and a much lower thermal gradient at the bottom surface of the enclosure. Moreover, when the circular cylinder is located at the vertical center of the enclosure, $\delta = 0$, the number of inner vortices for $Ra = 10^5$ is different than for $Ra = 10^4$, as shown in Figs. 5(b) and 6(b). Whereas there are four inner vortices for $Ra = 10^4$, there are two inner vortices at the upper half of the x-plane cross section of the enclosure for $Ra = 10^5$. Consequently, the dominant flow is in the upper half of the enclosure and the flow in the lower half of the enclosure is much weaker than that in the upper half. Thus, the thermal and flow fields are almost stratified in the lower region of the enclosure.

When the cylinder moves upward to $\delta = 0.15$, the thermal plume over the upper surface of the circular cylinder is divided into three plumes, as shown in Fig. 6(c). Two upwelling thermal plumes are generated over the upper surface of the inner circular cylinder. A third, weak, downward thermal plume appears on the top wall of the enclosure. Whereas the number of thermal plumes is changed at $\delta = 0.15$, the cores of the two main eddies are placed in the region above the halfway point of the circular cylinder, as shown in Fig. 6(c).

As δ increases further, the reduced space between the cylinder and the top wall of the enclosure confines the vertical motion of flow; as a result, heat conduction is locally predominant over convective heat transfer in this space. Even though there are three thermal plumes on the top of the surface of the cylinder, the cores of the two main eddies appear in the region below the halfway point of the circular cylinder, as shown in Figs. 6(d) and (e).

As the convection effect on heat transfer in the cubical enclosure increases, the thermal and flow fields on the z-plane cross section of the enclosure are distorted near the front and back walls of the enclosure, as shown in Figs. 6(f)-(j). This is because the effect of viscous shearing increases as the strength of local three-dimensional flow increases.

When the circular cylinder is placed at $\delta = -0.25$, three upward thermal plumes appear over the top surface of the inner circular cylinder, as shown in Fig. 6(f). As shown in Figs. 5(d) and 6(f), even though the strength of the plume at the longitudinal center of the top surface of the cylinder for $Ra = 10^5$ is weaker than that for $Ra = 10^4$, there are two

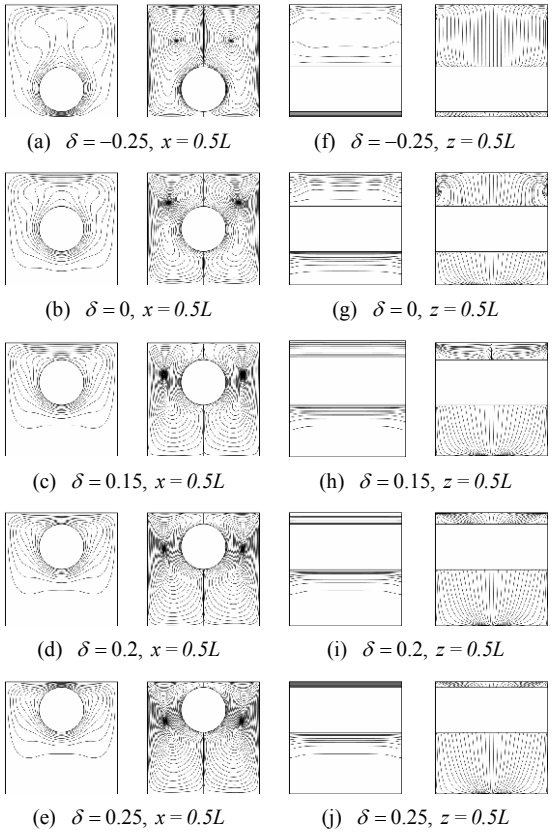

Fig. 6. Isotherms and streamlines for different δ values at $Ra = 10^5$ (contour values range from 0.1 to 1 with 10 levels).

thermal plumes near the front and back adiabatic walls of the cubical enclosure for $Ra = 10^5$, unlike the result for $Ra = 10^4$.

As the location of the circular cylinder approaches the vertical center of the cubical enclosure, the distance shortens between the two thermal plumes near the front and back walls of the enclosure. Eventually, when the circular cylinder is located at the vertical center of the enclosure, $\delta = 0$, there are just two upward thermal plumes over the top surface of the circular cylinder, as shown in Fig. 6(g). Owing to the increased effect of convection on the thermal and flow fields for $Ra = 10^5$, there is a weak upward thermal plume over the bottom wall of the enclosure, as shown in Fig. 6(g).

When the dimensionless location of the circular cylinder, δ, is greater than 0.15, as shown in Figs. 6(h)-(j), the isotherms over the top surface of the cylinder are stratified because of the narrow space between the cylinder and the top wall of the enclosure. However, there is still a thermal plume over the bottom wall of the enclosure.

3.1.4 $Ra = 10^6$

When Ra is 10^6, the distribution of thermal and flow fields in the cubical enclosure is influenced by buoyancy-induced convection, as shown in Fig. 7. Thus, the number of eddies on the x-plane cross section of the enclosure depends greatly on the location of the inner circular cylinder. In addi-

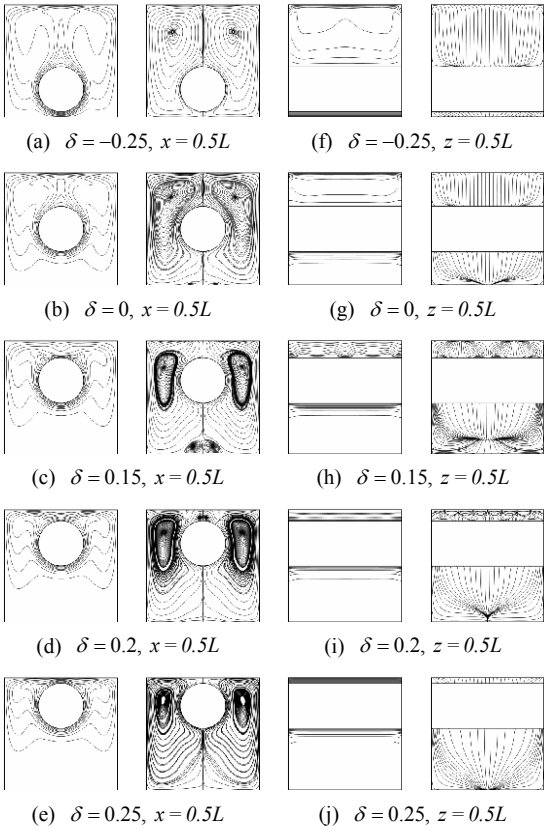

Fig. 7. Isotherms and streamlines for different δ values at $Ra = 10^6$ (contour values range from 0.1 to 1 with 10 levels).

tion to the different numbers of eddies on the x-plane cross section of the enclosure, the core of the two main eddies is placed at the region above the halfway point of the circular cylinder, regardless of the cylinder's location. This is because, as the Rayleigh number increases, the magnitude of the velocity circulating in the enclosure increases. As a result, the thermal boundary layer on the top wall of the enclosure for $Ra = 10^6$ becomes thinner than that for $Ra = 10^5$.

When the inner circular cylinder is located at $\delta = -0.25$, the thermal and flow fields on the x-plane cross section of the cubical enclosure for $Ra = 10^6$ have a similar pattern to that for $Ra = 10^5$. As shown in Figs. 6(a) and 7(a), when Ra is 10^6, the thermal plume over the upper surface of the cylinder strengthens, and the vertical location of the cores of the two main eddies is close to the top wall of the enclosure.

As the location of the circular cylinder nears the vertical center of the cubical enclosure, the pattern of isotherms for $Ra = 10^6$ is similar to that for $Ra = 10^5$. However, the streamlines on the x-plane cross section of the cubical enclosure show a different pattern in the space between the circular cylinder and the bottom wall of the enclosure. Whereas the streamlines on the bottom wall of the enclosure are almost parallel to the bottom wall for $Ra = 10^5$, as shown in Fig. 6(b), an upwelling pattern in the streamlines and two recirculating eddies appear at the center of the bottom wall for $Ra = 10^6$, as shown in Fig. 7(b).

As δ becomes higher than 0, the two recirculating eddies on the bottom wall of the cubical enclosure grow because of the increase in the convection effect and the space between the cylinder and the bottom wall of the enclosure. Similar to the result for $Ra = 10^5$, when the circular cylinder is placed at $\delta = 0.15$, there are three thermal plumes on the x-plane cross section of the enclosure owing to the narrow space between the cylinder and the top wall of the enclosure, as shown in Fig. 7(c). However, the two upward thermal plumes from the upper surface of the circular cylinder and the downward thermal plume from the top wall of the cubical enclosure for $Ra = 10^6$ are stronger than that for $Ra = 10^5$ owing to the increased effect of convection on thermal and fluid flow in the enclosure.

When the circular cylinder is placed at $\delta = 0.2$, four thermal plumes appear in the space between the cylinder and the top wall of the enclosure, as shown in Fig. 7(d). There are two upward plumes from the upper surface of the cylinder and two weak downward plumes from the top wall of the enclosure. In addition to the increased number of thermal plumes in the space between the cylinder and the top wall of the enclosure, two secondary vortices are newly generated over the upper surface of the cylinder, as shown in the streamline of Fig. 7(d). Whereas the two secondary vortices are generated in the space between the cylinder and the top wall of the enclosure, as shown in Fig. 7(d), the recirculating eddies disappear around the bottom wall of the enclosure owing to the increased space between the cylinder and the bottom wall.

The thermal field at $\delta = 0.25$ is similar to that at $\delta = 0.2$, as shown in Figs. 7(d)-(e). However, the two secondary vortices disappear in the space between the cylinder and the top wall of the enclosure, leaving just two main eddies on the x-plane cross section of the enclosure owing to the decreased space between the cylinder and the top wall.

When Ra is 10^6, the thermal and flow fields on the z-plane cross section of the enclosure are influenced by buoyancy-induced convection. Thus, the thermal and flow fields on the z-plane cross section of the enclosure at $Ra = 10^6$ display more complex patterns than those at $Ra = 10^5$, as shown in Figs. 7(f)-(j).

When the circular cylinder is located at $\delta = -0.25$, three upward thermal plumes over the top surface of the inner circular cylinder on the z-plane cross section of the enclosure for $Ra = 10^6$ are stronger than that for $Ra = 10^5$, as shown in Figs. 6(f) and 7(f). As the cylinder approaches the vertical center of the cubical enclosure, the plumes decrease at the longitudinal center of the cylinder. Eventually, when the circular cylinder is placed at the vertical center of the enclosure, $\delta = 0$, the thermal plume at the longitudinal center of the cylinder disappears and there are two thermal plumes around the front and back walls of the enclosure, as shown in Fig. 7(g). As shown in Figs. 6(g) and 7(g), the distance between the two thermal plumes for $Ra = 10^6$ is greater than that for $Ra = 10^5$. Additionally, the thermal boundary layer on the bottom surface of the circular cylinder for $Ra = 10^6$ is thinner

than that for $Ra = 10^5$. This is because the effects of buoyancy-induced convection and transverse rolls increase as the Rayleigh number increases.

When δ further increases to 0.15, five thermal plumes, four upward plumes, and one downward plume appear in the space between the cylinder and the top wall on the z-plane cross section of the enclosure, as shown in Fig. 7(h). There are four transverse rolls on the top surface of the circular cylinder. The number of transverse rolls increases when the circular cylinder is placed at $\delta = 0.2$, as shown in Fig. 7(i). However, there is no thermal plume in the space between the cylinder and the top wall of the enclosure owing to the narrow gap between the cylinder and the top wall. As the space narrows between the cylinder and the top wall of the enclosure, the effect of buoyancy-induced convection on the thermal and flow fields decreases in this region. Thus, when δ further increases to 0.25, there is no transverse roll or thermal plume in the space between the cylinder and the top wall of the enclosure, as shown in Fig. 7(j).

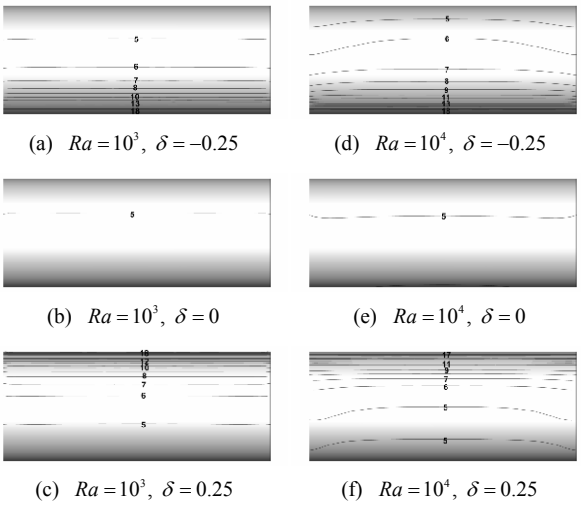

(a) $Ra = 10^3$, $\delta = -0.25$ (d) $Ra = 10^4$, $\delta = -0.25$

(b) $Ra = 10^3$, $\delta = 0$ (e) $Ra = 10^4$, $\delta = 0$

(c) $Ra = 10^3$, $\delta = 0.25$ (f) $Ra = 10^4$, $\delta = 0.25$

Fig. 8. Local Nusselt number distribution on the surface of the inner circular cylinder at different positions of the cylinder for $Ra = 10^3$ (left column, (a)-(c)) and $Ra = 10^4$ (right column, (d)-(f)).

3.2 Local Nusselt number of inner circular cylinder

Figs. 8 and 9 show the local distribution of Nusselt number on the surface of the circular cylinder, Nu_C, at different δ values for $Ra = 10^3$, 10^4, 10^5, and 10^6. Regardless of the location of the cylinder and the Rayleigh number, the thermal and flow fields in the cubical enclosure are symmetrical about the vertical center plane of the cubical enclosure, $z = 0.5L$. Thus, the distribution of Nu_C on the surface of the cylinder is visible in Figs. 8 and 9 from the right wall of the enclosure. As the Rayleigh number increases, the effect of three-dimensionality on the heat transfer between the cylinder and the enclosure grows. Thus, as the Rayleigh number increases, the difference increases between Nu_C at the longitudinal center of the cylinder and Nu_C around the two end walls of the cylinder.

When the circular cylinder is located at $\delta = -0.25$ for $Ra = 10^3$, the maximum value of Nu_C is at the bottom of the cylinder and the minimum value of Nu_C is at the top of the cylinder, as shown in Fig. 8(a). When δ further increases to 0, the value of Nu_C on the surface of the cylinder is nearly constant, as shown in Fig. 8(b). However, as the distance decreases between the cylinder and the top wall of the enclosure, the value of Nu_C at the upper part of the cylinder becomes higher than that at the bottom part of the cylinder. As a result, when the cylinder is placed at $\delta = 0.25$, the distribution of Nu_C is symmetrical to that at $\delta = -0.25$, as shown in Figs. 8(a) and (c). Regardless of δ, the distribution of Nu_C is almost parallel to the longitudinal direction of the cylinder, as shown in Figs. 8(a)-(c). In consequence, at this low Rayleigh number of 10^3, conduction is a dominant mode of heat transfer and the effect of three-dimensionality on the thermal and flow fields is negligible.

The maximum and minimum values of Nu_C for $Ra = 10^4$ are similar to those for $Ra = 10^3$. However, the distribution of Nu_C for $Ra = 10^4$ is unlike that for $Ra = 10^3$, as shown in Fig. 8. When the circular cylinder is located at $\delta = -0.25$, as shown in Fig. 8(d), Nu_C has an upwelling pattern at the longitudinal center of the cylinder because the effect of convection on the thermal and flow fields increases in the enclosure, as shown in Figs. 5(a) and (d). Thus, at the upper part of the cylinder, the value of Nu_C at the longitudinal center of the cylinder is higher than that around the two end walls of the cylinder. When $\delta = 0$, the value of Nu_C around the two end walls of the cylinder is slightly higher than that at the longitudinal center of the cylinder. However, the difference in the value of Nu_C is very small. When the circular cylinder is placed at $\delta = 0.25$, the minimum value of Nu_C does not exist at the lowest part of the cylinder. The minimum value of Nu_C appears between the vertical center and the lowest part of the cylinder, as shown in Fig. 8(f). This is because the intensity of circulating flow in the enclosure that impinges on the bottom of the cylinder for $Ra = 10^4$ is stronger than that for $Ra = 10^3$ owing to the increase in convection as the Rayleigh number increases. Thus, the position of the minimum local Nusselt number for $Ra = 10^4$ at $\delta = 0.25$ is not at the lowest part of the cylinder.

Fig. 9 shows the distribution of Nu_C at different locations of the cylinder for $Ra = 10^5$ and 10^6. The maximum value of Nu_C for $Ra = 10^5$ and 10^6 exists at the bottom of the cylinder, except in the cases of $\delta = 0.25$, because the thickness of the thermal boundary layer is the thinnest and the thermal gradient is the highest at the bottom of the cylinder.

When the value of δ is less than 0, for $Ra = 10^5$ and 10^6, the minimum value of Nu_C is at the highest part of the cylinder because the thermal boundary layer is thickest and the thermal gradient is lowest in this region. However, when the value of δ is higher than 0 (i.e., the circular cylinder is placed at the top of the enclosure), the position of the mini-

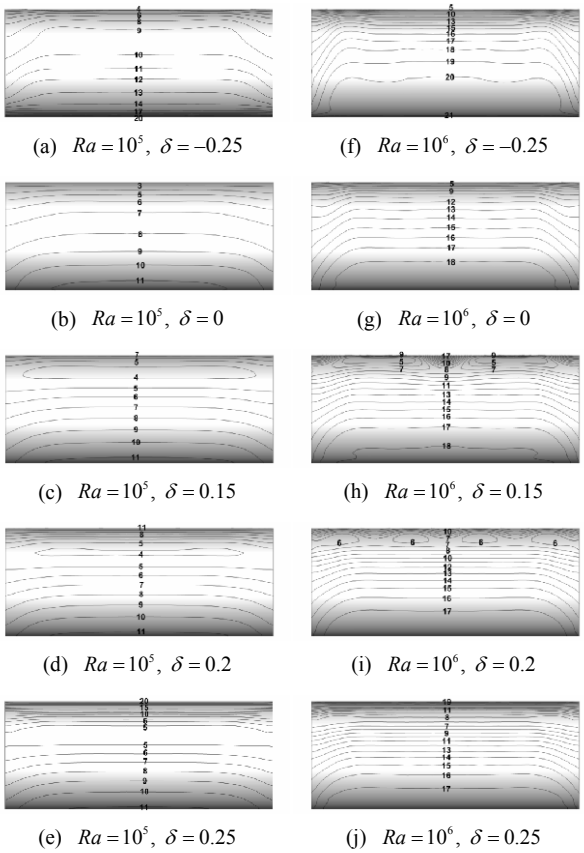

(a) $Ra = 10^5,\ \delta = -0.25$ (f) $Ra = 10^6,\ \delta = -0.25$

(b) $Ra = 10^5,\ \delta = 0$ (g) $Ra = 10^6,\ \delta = 0$

(c) $Ra = 10^5,\ \delta = 0.15$ (h) $Ra = 10^6,\ \delta = 0.15$

(d) $Ra = 10^5,\ \delta = 0.2$ (i) $Ra = 10^6,\ \delta = 0.2$

(e) $Ra = 10^5,\ \delta = 0.25$ (j) $Ra = 10^6,\ \delta = 0.25$

Fig. 9. Local Nusselt number distribution on the surface of the inner circular cylinder at different positions of the cylinder for $Ra = 10^5$ (left column, (a)-(e)) and $Ra = 10^6$ (right column, (f)-(j)).

mum Nu_C is not at the highest part of the cylinder, but is somewhere at the upper part of the cylinder owing to the strong interaction between the upward thermal plume and the available space between the cylinder and the top wall of the enclosure, depending on δ. Thus, as shown in Figs. 9(c), (d), (h) and (i), the position of the minimum value of Nu_C at $\delta = 0.15$ and 0.2 is identical to the position of thermal plumes over the surface of the circular cylinder.

3.3 Surface-averaged Nusselt number

Fig. 10(a) shows the surface-averaged Nusselt number on the top wall of the enclosure, $\overline{Nu}_T$, as a function of δ for different Rayleigh numbers. The value of $\overline{Nu}_T$ increases as the Rayleigh number increases, regardless of the location of the inner circular cylinder, owing to the increased effect of buoyancy-induced convection.

For $Ra = 10^3$ and 10^4, when the circular cylinder is placed at the lower half of the cubical enclosure, $\delta \le 0$, $\overline{Nu}_T$ increases slowly as δ increases. However, when the cylinder is located close to the top wall of the enclosure, the value of $\overline{Nu}_T$ increases very rapidly with increasing δ. The difference in the value of $\overline{Nu}_T$ between $Ra = 10^3$ and $Ra = 10^4$

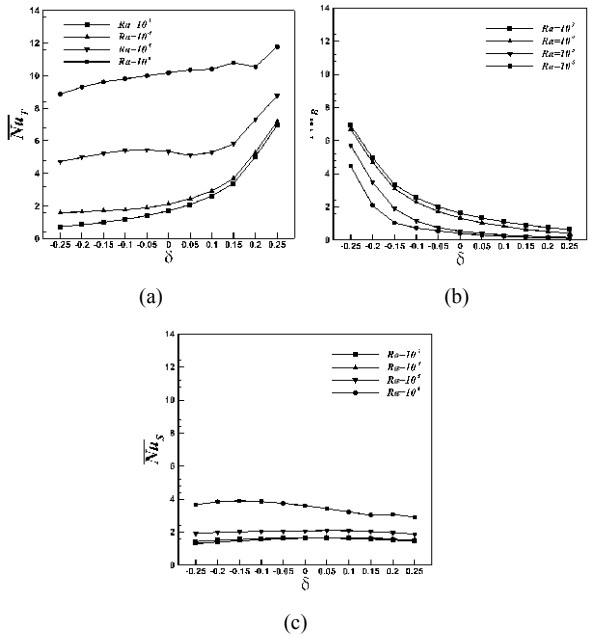

(a) (b)

(c)

Fig. 10. Surface-averaged Nusselt numbers as a function of δ for different Rayleigh numbers on (a) top wall; (b) bottom wall; (c) sidewall.

is highest at $\delta = -0.25$ and becomes constant when the value of δ is higher than 0.15, as shown in Fig. 10(a). This is because, as the space decreases between the cylinder and the top wall of the enclosure, the effect of convection on the thermal and flow fields in the enclosure decreases. Thus, when δ is higher than 0.15, conduction is a dominant mode of heat transfer between the circular cylinder and the top wall of the enclosure.

When δ increases from -0.25 to -0.05 at $Ra = 10^5$, as shown in Fig. 10(a), the value of $\overline{Nu}_T$ increases slowly because the thermal gradient on the top wall of the enclosure increases slightly as the distance decreases between the cylinder and the top wall. In this range of δ, the dependence of $\overline{Nu}_T$ on δ is very low. However, when δ increases to 0 and 0.05 at $Ra = 10^5$, the value of $\overline{Nu}_T$ decreases slightly as δ increases. This is because the strength of the upwelling thermal plume formed over the upper surface of the circular cylinder decreases and transverse rolls are formed on the top surface of the cylinder, as shown in Figs. 6(b) and (g). When δ further increases to 0.25, the effect of δ on $\overline{Nu}_T$ grows. However, the increase of $\overline{Nu}_T$ for $Ra = 10^5$ has a similar trend to that for $Ra = 10^3$ and $Ra = 10^4$ in the range of $0.1 \le \delta \le 0.25$. Thus, in this range of δ, the effect of convection on thermal and flow fields in the enclosure for $Ra = 10^5$ is not as dominant as the effect of conduction. This is because of the reduced space between the cylinder and the top wall of the enclosure with increasing δ.

When Ra is 10^6, the rate of increase in the value of $\overline{Nu}_T$ is the lowest with respect to the location of the cylinder, so the difference in the value of $\overline{Nu}_T$ between $\delta = -0.25$ and $\delta = 0.25$ is the smallest. This is because, when Ra is 10^6,

the effect of buoyancy-induced convection on the thermal and flow fields in the enclosure is dominant, even though the cylinder is placed close to the top wall of the enclosure. When δ increases from -0.25 to 0.15 at $Ra = 10^6$, as shown in Fig. 10(a), the value of $\overline{Nu}_T$ increases gradually. However, when the circular cylinder is placed at $\delta = 0.2$, the value of $\overline{Nu}_T$ decreases because of the strong interaction between the secondary vortices and the transverse rolls, as shown in Figs. 7(d) and (i). When $\delta = 0.25$ at $Ra = 10^6$, the value of $\overline{Nu}_T$ increases again to the maximum value. This is because the effect of conduction on heat transfer between the inner circular cylinder and the top wall of the enclosure increases when the distance between the cylinder and the top wall is the smallest.

Fig. 10(b) shows the surface-averaged Nusselt number on the bottom wall of the cubical enclosure, $\overline{Nu}_B$, as a function of δ for different Rayleigh numbers. Regardless of the Rayleigh number, the value of $\overline{Nu}_B$ decreases with increasing δ. The dependence of $\overline{Nu}_B$ on δ is generally higher than that of $\overline{Nu}_T$. When $-0.25 \le \delta \le 0$, the value of $\overline{Nu}_B$ decreases very rapidly with increasing δ. In this range of δ, the value of $\overline{Nu}_B$ is highly dependent on δ, regardless of Ra. However, when $0 \le \delta \le 0.25$, the value of $\overline{Nu}_B$ decreases slowly with increasing δ. This is because the variation of isotherms in the stagnation flow region is slow when the circular cylinder is placed in the range of $0 \le \delta \le 0.25$.

Fig. 10(c) shows the surface-averaged Nusselt number on the sidewall of the enclosure, $\overline{Nu}_S$, as a function of δ for different Rayleigh numbers. The value of $\overline{Nu}_S$ generally increases as the Rayleigh number increases because the effect of convection on heat transfer between the cylinder and the enclosure increases. However, the dependence of $\overline{Nu}_S$ on δ is very low, unlike the cases of $\overline{Nu}_T$ and $\overline{Nu}_B$. Whereas the effect of δ on the value of $\overline{Nu}_S$ is negligible for $10^3 \le Ra \le 10^5$, the value of $\overline{Nu}_S$ decreases generally as δ increases for $Ra = 10^6$. This is because the effect of convection on heat transfer on the sidewall of the enclosure decreases as δ increases.

Fig. 11 shows the total surface-averaged Nusselt number of the enclosure, $\overline{Nu}_{EN}$, and the surface-averaged Nusselt number of the circular cylinder, $\overline{Nu}_C$, as a function of δ for different Rayleigh numbers. When $Ra = 10^3$ and 10^4, the value of $\overline{Nu}_{EN}$ has a parabolic profile with the minimum value at $\delta = 0$. The value of $\overline{Nu}_{EN}$ for $Ra = 10^4$ is almost the same as that for $Ra = 10^3$, regardless of δ. However, when Ra is 10^5, the minimum value of $\overline{Nu}_{EN}$ is at $\delta = 0.05$, and the value of $\overline{Nu}_{EN}$ at $\delta = -0.25$ is higher than that at $\delta = 0.25$, as shown in Fig. 11(a). This is because the effect of convection on the heat transfer between the cylinder and the enclosure increases as the Rayleigh number and the space between the cylinder and the top wall of the enclosure increase. When Ra increases to 10^6, the minimum value of $\overline{Nu}_{EN}$ is $\delta = 0.2$, as shown in Fig. 11(a). The difference between the minimum value of $\overline{Nu}_{EN}$ and the second lowest value of $\overline{Nu}_{EN}$ for $Ra = 10^6$ is greater than that for

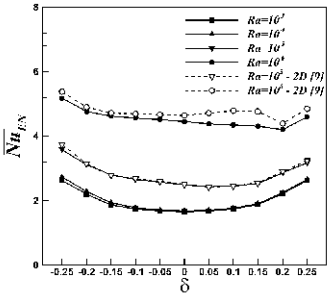

(a)

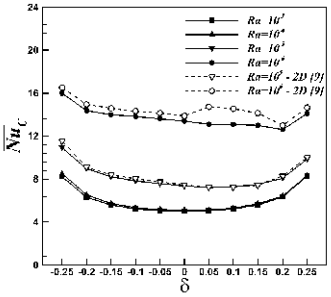

(b)

Fig. 11. Total (a) surface-averaged Nusselt number of enclosure, $\overline{Nu}_{EN}$, and; (b) surface-averaged Nusselt number of the inner cylinder, $\overline{Nu}_C$, as a function of δ for different Rayleigh numbers. Two-dimensional results were obtained by Kim et al. [9].

$Ra = 10^5$. This is because the decrease in the value of $\overline{Nu}_{EN}$ for $Ra = 10^6$ is caused by the strong interaction between the secondary vortices and the transverse rolls, as shown in Figs. 7(d) and (i). The pattern of variation of $\overline{Nu}_C$ as a function of δ is generally similar to that of $\overline{Nu}_{EN}$, as shown in Fig. 11(b).

When $10^3 \le Ra \le 10^4$, the effect of three-dimensionality on the thermal and flow fields in the enclosure is negligible. However, as shown in Fig. 11, when $10^5 \le Ra \le 10^6$, $\overline{Nu}_{EN}$ and $\overline{Nu}_C$ obtained in this study are different from those obtained by Kim et al. [9] using a two-dimensional calculation owing to the increase in the three-dimensionality effect. As the Rayleigh number increases, the difference in the value of $\overline{Nu}_{EN}$ and $\overline{Nu}_C$ increases between the three-dimensional and two-dimensional calculation results. When $Ra = 10^5$, the maximum difference occurs at $\delta = -0.25$. When the circular cylinder is located in the range of $-0.2 \le \delta \le 0.25$, the value of $\overline{Nu}_{EN}$ and $\overline{Nu}_C$ for the three-dimensional calculation is similar to that for the two-dimensional calculation. However, when $Ra = 10^6$, the value of $\overline{Nu}_{EN}$ and $\overline{Nu}_C$ for the three-dimensional calculation is less than that for the two-dimensional calculation owing to the effect of three-dimensionality on heat transfer between the cylinder and the enclosure. The maximum difference occurs at $0.05 \le \delta \le 0.15$ because the recirculating eddies and transverse rolls appear in the enclosure. In the range of $0.05 \le \delta \le 0.15$, the value of $\overline{Nu}_{EN}$ and $\overline{Nu}_C$ for the three-dimensional calculation is approximately 10 percent less than that for the two-

dimensional calculation.

4. Conclusions

The present study investigates the effects of a high-temperature inner circular cylinder, present at different locations along the vertical centerline of a low-temperature cubical enclosure, on fluid flow and heat transfer for different Rayleigh numbers in the range of $10^3 \le Ra \le 10^6$. The IBM is implemented with a finite-volume method to simulate three-dimensional flow and heat transfer over the cylinder in the cubical enclosure in Cartesian coordinates.

For different locations of the inner cylinder and different values of the Rayleigh number, the thermal and flow field characteristics change. However, for all Rayleigh numbers considered in this study, the thermal and flow fields eventually reach steady state. When Ra is 10^3, three-dimensionality in the thermal and flow fields due to the front and back walls of the cubical enclosure does not exist for any locations of the inner cylinder. As the Rayleigh number increases, the effect of three-dimensionality grows of the front and back walls of the enclosure on the thermal and flow fields in the cubical enclosure. In particular, the effect of three-dimensionality in the thermal and flow fields on the heat transfer between the cylinder and the enclosure is great when the inner cylinder is located at the lower half of the cubical enclosure. This is because the space between the cylinder and the top wall of the enclosure is secure when the inner cylinder is located at the lower half of the enclosure. When Ra is 10^6, even though the space between the cylinder and the top wall of the enclosure narrows, the pattern appears of thermal and flow fields attributable to the effect of the front and back walls of the enclosure because the effect of buoyancy-induced convection is predominant over the effect of conduction. Thus, when $Ra = 10^6$, complex thermal and flow patterns exist with respect to the location of the inner cylinder, δ.

The change in thermal and flow patterns in the space between the cylinder and the enclosure with respect to δ and Ra has an influence on the distribution of the Nusselt number on the surface of the cylinder and walls of the enclosure. As the Rayleigh number increases, the effect of δ on the distribution of Nusselt number on the surface of the cylinder and walls of the enclosure increases. For $Ra = 10^5$ and 10^6, the maximum surface-averaged Nusselt number of the cylinder and enclosure occurs when the circular cylinder is located at $\delta = -0.25$. This is because the wide space between the cylinder and the top wall of the enclosure ensures the strong circulation of flow. However, the location of the cylinder for the minimum surface-averaged Nusselt number of the cylinder and enclosure depends on the Rayleigh number because the strength of the local three-dimensional flow increases as the Rayleigh number increases. As the Rayleigh number increases, the difference in the value of $\overline{Nu}_{EN}$ and $\overline{Nu}_{C}$ increases between the three-dimensional and two-dimensional calculations. When the circular cylinder is located in the range of $0.05 \le \delta \le 0.15$ for $Ra = 10^6$, the difference due to three-dimensionality is at its maximum. The maximum difference in this range of δ for $Ra = 10^6$ is about 10 percent.

Acknowledgment

This research was supported by Leading Foreign Research Institute Recruitment Program through the National Research Foundation of Korea(NRF) funded by the Ministry of Science, ICT & Future Planning(No.2009-00495), and also by the National Research Foundation of Korea(NRF) grant funded by the Korea government(MSIP) (No.2013R1A2A2A01067251). Further support of this work was provided by PLSI supercomputing resources of Korea Institute of Science and Technology Information.

References

[1] N. Quertatani, N. B. Cheikh, B. B. Beya and T. Lili, Numerical simulation of two-dimensional Rayleigh-Bénard convection in an enclosure, *Comptes Rendus Mecanique*, 336 (2008) 464-470.

[2] M. C. D'Orazio, C. Cianfrini and M. Corcione, Rayleigh-Bénard convection in tall rectangular enclosures, *Int. J. Thermal Sci.*, 43 (2004) 135-144.

[3] M. Corcione, Effects of the thermal boundary conditions at the sidewalls upon natural convection in rectangular enclosures heated from below and cooled from above, *Int. J. Thermal Sci*., 42 (2003) 199-208.

[4] A. Valencia and R. L. Frederick, Heat transfer in square cavities with partially active vertical walls, *Int. J. Heat Mass Transfer*, 32 (8) (1989) 1567-1574.

[5] J. M. Hyun and J. W. Lee, Numerical solutions for transient natural convection in a square cavity with different sidewall temperatures, *Int. J. Heat and Fluid Flow*, 10 (2) (1989) 146-151.

[6] G. Cesini, M. Paroncini, G. Cortella and M. Manzan, Natural convection from a horizontal cylinder in a rectangular cavity, *Int. J. Heat Mass Transfer*, 42 (1999) 1801-1811.

[7] C. Shu and Y. D. Zhu, Efficient computation of natural convection in a concentric annulus between an outer square cylinder and an inner circular cylinder, *Int. J. Numer. Methods in Fluids*, 38 (2002) 429-445.

[8] D. Angeli, P. Levoni and G. S. Barozzi, Numerical predictions for stable buoyant regimes within a square cavity containing a heated horizontal cylinder, *Int. J. Heat Mass Transfer*, 51 (2008) 553-565.

[9] B. S. Kim, D. S. Lee, M. Y. Ha and H. S. Yoon, A numerical study of natural convection in a square enclosure with a circular cylinder at different vertical locations, *Int. J. Heat Mass Transfer*, 51 (2008) 1888-1906.

[10] X. Xu, Z. Yu, Y. Hu, L. Fan and K, Cen, A numerical study of laminar natural convective heat transfer around a horizontal cylinder inside a concentric air-filled triangular enclosure, *Int. J. Heat Mass Transfer*, 53 (2010) 345-355.

[11] A. M. C. Chan and S. Banerjee, A numerical study of three-dimensional roll cells within rigid boundaries, *J. Heat Transfer*, 101 (2) (1979) 233-243.
[12] T. Fusegi, J. Hyun, K. Kuwahara and B. Farouk, A numerical study of three-dimensional natural convection in a differentially heated cubical enclosure, *Int. J. Heat Mass Transfer,* 34 (1991) 1543-1557.
[13] J. Pallares, I. Cuesta, F. Grau and F. Giralt, Natural convection in a cubical cavity heated from below at low Rayleigh numbers, *Int. J. Heat Mass Transfer*, 39 (1996) 3233-3247.
[14] M. Y. Ha and M. J. Jung, A numerical study of three-dimensional conjugate heat transfer of natural convection and conduction in a differentially heated cubic enclosure with a heat-generating cubic conducting body, *Int. J. Heat Mass Transfer*, 43 (2000) 4229-4248.
[15] H. S. Yoon, D. H. Yu, M. Y. Ha and Y. G. Park, Three-dimensional natural convection in an enclosure with a sphere at different vertical locations, *Int. J. Heat Mass Transfer*, 53 (15-16) (2010) 3143-3155.
[16] J. M. Lee, M. Y. Ha and H. S. Yoon, Natural convection in a square enclosure with a circular cylinder at different horizontal and diagonal locations, *Int. J. Heat Mass Transfer*, 53 (2010) 5905-5919.
[17] D. H. Kang, M. Y. Ha, H. S. Yoon and C. Choi, Bifurcation to unsteady natural convection in square enclosure with a circular cylinder at Rayleigh number of 10^7 , *Int. J. Heat Mass Transfer*, 64 (2013) 926-944.
[18] H. S. Yoon, M. Y. Ha, B. S. Kim and D. H. Yu, Effect of the position of a circular cylinder in a square enclosure on natural convection at Rayleigh number of 10^7 , *Physics of Fluids*, 21 (2009) 047101.
[19] Y. G. Park, M. Y. Ha and H. S. Yoon, Study on natural convection in a cold square enclosure with a pair of hot horizontal cylinders positioned at different vertical locations, *Int. J. Heat Mass Transfer*, 65 (2013) 696-712.
[20] J. Kim, D. Kim and H. Choi, An immersed-boundary finite volume method for simulations of flow in complex geometries, *J. Comput. Phys*., 171 (2001) 132-150.
[21] J. Kim and H. Choi, An immersed-boundary finite-volume method for simulation of heat transfer in complex geometries, *KSME Int. J*., 18 (2004) 1026-1035.
[22] D. Fiscaletti, D. Angeli, L. Tarozzi and G. S. Barozzi, Buoyancy-induced transitional flows around an enclosed horizontal cylinder: an experiment, *Int. J. Heat Mass Transfer*, 58 (2013) 619-631.

Man-Yeong Ha received his B.S. degree from Pusan National University, Korea, in 1981, M.S. degree, in 1983, from Korea Advanced Institute of Science and Technology, Korea, and Ph.D. from Pennsylvania State University, USA in 1990. Dr. Ha is currently a Professor at the School of Mechanical Engineering at Pusan National University in Busan, Korea. He serves as an Editor of the Journal of Mechanical Science and Technology. His research interests are focused on thermal management, computational fluid dynamics, and micro/ nano fluidics.

Changyoung Choi received his B.S., M.S. and Ph.D. degrees from Pusan National University, Korea, in 2008, 2010 and 2014, respectively. In his master and doctoral course, he conducted many researches under the supervision of Prof. Man-Yeong Ha. His research interests are focused on flow analysis and control in turbulent flows and thermo-fluid phenomena analysis for enhancing the efficiency of the industrial devices.